Congresso de Métodos Numéricos em Engenharia 2015
Lisboa, 29 de Junho a 2 de Julho 2015

PENALTY-PROJECTION METHOD FOR A MONOLITHIC FLUID STRUCTURE INTERACTION SOLVER

D. Cerroni*, S. Manservisi and F. Menghini.

DIN-University of Bologna
Laboratory of Montecuccolino, Via dei Colli 16, Bologna 40136, Italy
(*) e-mail: daniele.cerroni2@unibo.it

Keywords: Fluid Structure Interaction, Penalty-Projection algorithm, Monolithic solver

Abstract. *In this paper we present the results of Fluid-Structure Interaction (FSI) computations of an incompressible solid object and laminar incompressible viscous flows using a combined penalty-projection algorithm. The system consists of a fluid region governed by Navier-Stokes equations and a solid domain described by elastic and hyperelastic structure mechanical equations. In particular we impose the incompressibility constraint both in the solid hyperelastic and incompressible fluid region by using an iterative projection method which decouples pressure and velocity field. This technique reduces the degrees of freedom of the problem decreasing the computational cost of the solution algorithm. However in the projection pressure equation is not possible to impose the physical boundary conditions and consistent errors are generated on the solid boundary. In order to correct this boundary error due to the decoupling projection algorithm a combined projection-penalty method is introduced. The fluid and the solid incompressibility constraint are imposed in a monolithic approach over all the fluid and solid unknowns when large displacement occurs. In order to verify the accuracy of the proposed method we compare the results of the projection with the projection-penalty and coupled algorithm. These analyzed cases show stability and robustness of the proposed algorithm for appropriate value of the penalty parameter together with a reduction of the computational effort compared with that needed by the coupled algorithm.*

1 INTRODUCTION

In the last decades the interest in the study of Fluid-Structure interaction problems has been increasing because of the huge number of applications in various fields of engineering. Some examples are the stability and response of aircraft wings, the flow of blood through arteries, the response of bridges and tall buildings to winds, the vibration of turbine and compressor blades and the oscillation of heat exchangers (e.g., see [1, 2, 3, 4]). In particular, concerning the biological field, the fluid structure interaction is of great interest because of the increasing demand in the medical community for scientifically rigorous

and quantitative investigations of cardiovascular diseases. A fluid structure interaction problem consists in solving the mass and the continuum balance equations for a system composed of fluid and solid components. The most commonly solution strategy encountered and implemented in software packages is the so-called partitioned approach, which decouples the fluid-solid problem into two separate sub-problems and uses dedicated software for the solution [5]. According to this solution strategy the coupling between the two physical domains is achieved with a boundary condition to be enforced at the interface between the fluid and the solid domain. In applications where large displacements occur, such as in the hemodynamics field, explicit partitioned algorithms show instabilities and convergence problems since the coupling conditions are not exactly enforced leading to unbalanced displacement and velocity fields at the interface. In these cases numerical experiments show that only fully coupled or monolithic algorithms exhibit excellent stability properties [6, 7] since they implicitly enforce the coupling condition at each time step. The monolithic algorithm solves simultaneously the fluid and the structure unknowns in a unique solver so that the solid and fluid regions are treated as a single continuum and the boundary conditions at the interface are automatically enforced [2, 8]. Monolithic fully-coupled algorithms are always stable in the energy norm but they are also CPU-time expensive. This issue is enhanced by the saddle-point character of the incompressible solid and fluid formulation and it may be of particular importance in three-dimensional geometries where a high number of degrees of freedom has to be managed.

Reduction of the computational cost for FSI problems is the main motivation of this work. This purpose is achieved by splitting the computation of the velocity and the pressure by using a projection method. The method consists of two steps: a predictor and a corrector step. In a first predictor step, it is computed an intermediate velocity which does not satisfy the divergence constraint. This velocity is projected onto a divergence-free space in a subsequent pressure correction stage [9, 10]. In such way a mathematical decoupling of the computation of velocity and pressure is performed over the whole solid and fluid domain allowing reduction of the oscillations induced by the domain partitioning in the enforcement of the interface conditions. In order to enforce stress-free boundary conditions a penalty method must also be taken into account. The idea we propose is to couple the iterative projection algorithm proposed by Chorin and Temam together with a penalty algorithm ensuring proper boundary conditions.

The paper is organized as follows. In the next section we recall the general balance equations in the ALE formulation and a monolithic description of the Fluid-Structure Interaction problem. We also introduce the continuous FSI weak formulation together with the proposed iterative-penalty-projection algorithm. The numerical results are reported in section 4 showing the differences between a standard projection method and the iterative-penalty-projection explaining the importance of the correction provided by the penalty. All the simulations are performed using an object oriented, parallel finite element code. Finally we draw our conclusion and some proposals for the evolution of the work.

2 FLUID STRUCTURE INTERACTION PROBLEM

2.1 CONTINUUM DESCRIPTION

In this section we introduce the notation used to describe current and reference config-

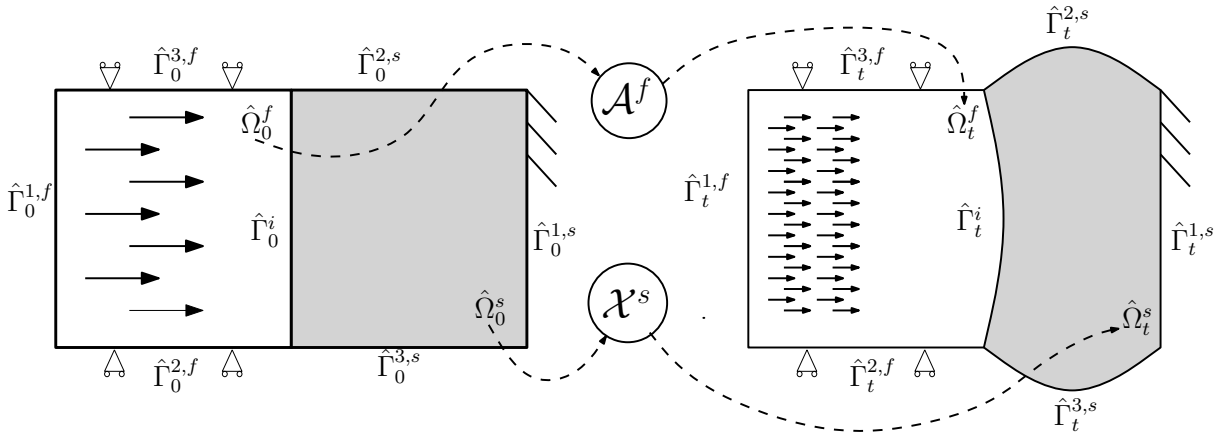

Figure 1: Reference and current deformed configurations for a generic FSI domain.

uration in fluid and solid domain. In an ordinary FSI problem we consider a mechanical system composed by a laminar Newtonian fluid region and a solid one which defines a moving domain Ω_t. A schematic geometry of the problem is shown in Figure 1. Let Ω_t^f and Ω_t^s be the fluid and the solid region at $t \in (0, T]$, respectively. At $t = 0$ the fluid and solid region are defined by $\hat{\Omega}_0^f$ and $\hat{\Omega}_0^s$. Let $\Gamma_t^i = \bar{\Omega}_t^f \cap \bar{\Omega}_t^s$ and $\hat{\Gamma}_0^i = \bar{\Omega}_0^f \cap \bar{\Omega}_0^s$ be the interface where solid and fluid interact. $\Gamma_t^k, k = 1, 2, 3$ and $\hat{\Gamma}_0^k, k = 1, 2, 3$ are defined to be the remaining external boundaries at $t \in (0, T]$ and $t = 0$, respectively. The evolution of the solid and fluid domain $\hat{\Omega}_0^f$ and $\hat{\Omega}_0^s$ are defined by

$$\mathcal{X}^s : \hat{\Omega}_0^s \times \mathbb{R}^+ \to \mathbb{R}^3 ,$$
$$\mathcal{A}^f : \hat{\Omega}_0^f \times \mathbb{R}^+ \to \mathbb{R}^3 ,$$

such that the range of $\mathcal{X}^s(\cdot, t)$ and $\mathcal{A}^f(\cdot, t)$ define Ω_t^s and Ω_t^f, respectively. $\mathcal{X}^s$ maps any material point $\hat{\mathbf{x}}_0^s$ from the given fixed reference configuration $\hat{\Omega}_0^s$ to the current solid material configuration Ω_t^s. The solid displacement is then defined as

$$\hat{\mathbf{u}}^s(\hat{\mathbf{x}}_0^s, t) = \mathcal{X}(\hat{\mathbf{x}}_0^s, t) - \hat{\mathbf{x}}_0^s . \tag{1}$$

The mapping $\mathcal{A}^f$ is such that $\mathcal{A}^f(\hat{\mathbf{x}}_0^f, t) = \hat{\mathbf{x}}_0^f + \hat{\mathbf{u}}^f(\hat{\mathbf{x}}_0^f, t)$, where $\hat{\mathbf{u}}^f(\hat{\mathbf{x}}_0^f, t)$ is defined as an arbitrary extension operator over the fluid domain $\hat{\Omega}_0^f$ and given by

$$\hat{\mathbf{u}}^f(\hat{\mathbf{x}}_0^f, t) = \mathrm{Ext}(\hat{\mathbf{u}}^s|_{\hat{\Gamma}_0^i}) \quad \text{in} \quad \hat{\Omega}_0^f . \tag{2}$$

For details one can see [11, 12]. The extension operator more commonly used to evaluate the fluid region displacement is the harmonic or Laplace operator, other employed operators can be found in [13]. In our case the fluid displacement $\hat{\mathbf{u}}^f$ is defined by the solution of the following elliptic problem

$$\begin{aligned} \frac{\partial \hat{\mathbf{u}}^f}{\partial t} - k\Delta \hat{\mathbf{u}}^f = 0 \qquad & \text{in} \quad \hat{\Omega}_0^f \,, \\ \hat{\mathbf{u}}^f = \hat{\mathbf{u}}^s \qquad & \text{on} \quad \hat{\Gamma}_0^i \,, \end{aligned} \tag{3}$$

where k is the diffusion coefficient [11, 14, 15]. Other choices of the extension operator can be used, for details one can see [13].

Now we can define the velocity $\mathbf{w}^f$ of the fluid domain points in the current configuration. The velocity $\hat{\mathbf{w}}^f$ is defined by

$$\hat{\mathbf{w}}^f = \frac{\partial \hat{\mathbf{u}}^f}{\partial t} \quad \text{in} \quad \hat{\Omega}_0^f \,. \tag{4}$$

This quantity represents the velocity in terms of the reference coordinate $\hat{\mathbf{x}}_0^f$.

2.2 THE FLUID PROBLEM

The behavior of the fluid is described by the Navier-Stokes equations for incompressible flows

$$\begin{aligned} & \rho^f \frac{\partial \mathbf{v}^f}{\partial t}\bigg|_{\tilde{\mathcal{A}}} + \rho^f \left(\mathbf{v}^f - \mathbf{w}^f\right) \cdot \nabla \mathbf{v}^f - \nabla \cdot \sigma^f = \mathbf{0} && \text{in} \quad (0,T) \times \Omega_t^f \,, \\ & \nabla \cdot \mathbf{v}^f = \mathbf{0} && \text{in} \quad (0,T) \times \Omega_t^f \,, \\ & \mathbf{v}^f|_{t=0} = \mathbf{v}_0 && \text{in} \quad \hat{\Omega}_0^f \,, \\ & \mathbf{v}^f|_{\Gamma_{t,D}^{1,f} \cup \Gamma_{t,D}^{2,f}} = \mathbf{g}^f && \text{in} \quad (0,T) \,, \\ & \sigma_f \cdot \mathbf{n}^f|_{\Gamma_{t,N}^{1,f} \cup \Gamma_{t,}^{2,f}} = \mathbf{h}^f && \text{in} \quad (0,T) \,. \end{aligned} \tag{5}$$

where ρ^f is the constant density, $\mathbf{v}^f$ is the fluid velocity, $\tilde{\mathcal{A}}$ denotes the ALE application that maps the reference fluid configuration $\hat{\Omega}_0^f$ onto the current fluid configuration Ω_t^f and $\mathbf{w}^f$ denotes the fluid domain velocity. $\mathbf{n}$ is the unit normal vector that points outward from the boundary $\partial\Omega_t^f$ and $\mathbf{g}^f$, $\mathbf{h}^f$, $\mathbf{v}_0$ are given data. The variables constituting the state of the flow in the incompressible case are the pressure p^f and the velocity $\mathbf{v}^f$. The contribution of external forces like gravity is assumed to be negligible. The constitutive relation for the stress tensor in the Newtonian incompressible case reads

$$\sigma^f = -p^f \mathbf{I} + \tau^f = -p^f \mathbf{I} + 2\mu^f \epsilon\left(\mathbf{v}^f\right) \,, \tag{6}$$

where μ^f is the dynamic viscosity of the fluid, p^f the Lagrange multiplier associated to the incompressibility constraint and $\epsilon\left(\mathbf{v}^f\right)$ the strain rate tensor defined as

$$\epsilon\left(\mathbf{v}^f\right) = \frac{1}{2}\left(\nabla \mathbf{v}^f + \left(\nabla \mathbf{v}^f\right)^{\mathrm{t}}\right) \,. \tag{7}$$

The total time derivative is related to the adopted reference systems.

2.3 THE SOLID PROBLEM

The governing equations for structural mechanics are the following momentum equations

$$\rho^s \left(\frac{\partial \mathbf{v}^s}{\partial t} + \mathbf{v}^s \cdot (\nabla \mathbf{v}^s) \right) - \nabla \cdot \sigma^s(\mathbf{u}^s) = \mathbf{0} \qquad \text{in} \quad \Omega_t^s \,, \tag{8}$$

where ρ^s is the density of the material, $\mathbf{v}^s$ is the velocity field and σ^s is the Cauchy stress tensor, which is a function of the displacement $\mathbf{u}^s$ of the structure. Since the constitutive law for the solid stress tensor is expressed in terms of displacements one must solve both the balance equations (8) and the kinematic relation

$$\mathbf{v}^s = \frac{\partial \mathbf{u}^s}{\partial t} \,. \tag{9}$$

For the reference configuration we can introduce the right Cauchy-Green deformation tensor $\mathbf{C}$ as

$$\mathbf{C} = \mathbf{F}^{\mathrm{t}} \cdot \mathbf{F} \,, \tag{10}$$

where $\mathbf{F}$ is the deformation gradient tensor defined by $\mathbf{F} = \mathbf{I} + \nabla \mathbf{u}^s$. In a similar way in the current configuration we can introduce the left Cauchy-Green deformation tensor, $\mathbf{b}$, as

$$\mathbf{b} = \mathbf{F} \cdot \mathbf{F}^{\mathrm{t}} \,. \tag{11}$$

According with this notation we can now express the Cauchy stress tensor, σ^s , as [14]

$$\sigma_{ij}^s = \frac{2}{J} \begin{bmatrix} b_{ij} & (\mathbf{I} b_{ij} - b_{im} b_{mj}) & \dfrac{J \delta_{ij}}{2} \end{bmatrix} \begin{pmatrix} \frac{\partial W}{\partial I} \\ \\ \frac{\partial W}{\partial II} \\ \\ \frac{\partial W}{\partial J} \end{pmatrix} \tag{12}$$

where $I = \mathrm{tr}\,\mathbf{C}$, $II = \mathrm{tr}\,(\mathbf{C}^2) - (\mathrm{tr}\,\mathbf{C})^2$ are the first and second invariant of the right Cauchy-Green strain tensor $\mathbf{C}$ and J its determinant. The quantity $W = W(I, II, J)$ is the strain energy of the system which depends on the constitutive law of the considered material. For example for a Neo-Hookian material, with respect to the current configuration, the energy function is defined by

$$\begin{aligned} W(I,J) = & \frac{1}{2}\mu_s \left(J^{-2/3} \mathrm{tr}\mathbf{C} - 3 \right) + \\ & \frac{1}{2} \left(\lambda + \frac{2}{3}\mu_s \right) \left(\frac{1}{2}(J^2 - 1) - \ln J \right) \,. \end{aligned} \tag{13}$$

In the case of incompressible solid the third invariant is equal to one so the energy density function becomes

$$W(I,J) = \frac{1}{2}\mu_s \left(\mathrm{tr}\mathbf{C} - 3\right). \tag{14}$$

and the Cauchy stress tensor is defined by

$$\sigma^s = -p^f \mathbf{I} + \sigma^{s*} \tag{15}$$

where σ^{s*} is the tensor obtained by using the equations (12) and (14).

2.4 THE COUPLED FLUID-STRUCTURE PROBLEM

The problem defined by (5)-(8) is not well posed since we have not yet prescribed any boundary conditions at the interface Γ_t^i. The coupling between the fluid and the solid model determines the missing boundary conditions, which consist of imposing the continuity of velocity and stress at the interface Γ_t^i in the following form

$$\mathbf{v}^f|_{\Gamma_t^i} = \mathbf{v}^s|_{\Gamma_t^i}, \tag{16}$$

$$\sigma^f \cdot \mathbf{n}^f|_{\Gamma_t^i} + \sigma^s \cdot \mathbf{n}^s|_{\Gamma_t^i} = \mathbf{0}. \tag{17}$$

To write the weak formulation of the coupled problem, let us consider the following functional spaces

$$\begin{aligned}
\mathbf{V}^t &= \{\phi \in \mathbf{H}^1(\Omega_t^f) : \phi|_{\Gamma_{t,D}^{1,f} \cup \Gamma_{t,D}^{2,f}} = \mathbf{0}\}, \\
\mathbf{V}_g^t &= \{\phi \in \mathbf{H}^1(\Omega_t^f) : \phi|_{\Gamma_{t,D}^{1,f} \cup \Gamma_{t,D}^{2,f}} = \mathbf{g}^f\}, \\
\mathbf{Q}^t &= L^2(\Omega_t^f), \\
\mathbf{M}^0 &= \{\psi \in \mathbf{H}^1(\hat{\Omega}_0^s) : \psi|_{\hat{\Gamma}_{0,D}^{1,s} \cup \hat{\Gamma}_{0,D}^{2,s} \cup \hat{\Gamma}_{0,D}^{3}} = \mathbf{0}\}, \\
\mathbf{M}_g^0 &= \{\psi \in \mathbf{H}^1(\hat{\Omega}_0^s) : \psi|_{\hat{\Gamma}_{0,D}^{1,s} \cup \hat{\Gamma}_{0,D}^{2,s} \cup \hat{\Gamma}_{0,D}^{3}} = \mathbf{g}^s\}, \\
\mathbf{D}^0 &= L^2(\hat{\Omega}_0^s).
\end{aligned}$$

In addition, let us introduce the following bilinear form

$$a^f(\mathbf{v}^\mathbf{f}, \phi) = \mu(\nabla \mathbf{v}^f + (\nabla \mathbf{v}^f)^T, \nabla \phi) \tag{18}$$

where we denote with $(\cdot,\cdot)$ the $L^2(\Omega_t^f)$ inner product. The variational formulation of the fluid equations can be obtained through the usual method by multiplying the equations (5) with appropriate test functions, performing integrations on the whole domain and keeping into account the boundary and interface conditions. This procedure leads at each

time t, for the velocity field $\mathbf{v} \in \mathbf{V}_g^t$ and pressure $p \in Q^t$, to the following weak formulation

$$\begin{aligned}
&\rho^f(\frac{\partial \mathbf{v}^f}{\partial t}\Big|_{\tilde{\mathcal{A}}}, \phi) + a(\mathbf{v}^f, \phi) - \rho^f((\nabla \cdot \mathbf{w}^f)\mathbf{v}^f, \phi) + \rho^f(\left(\mathbf{v}^f - \mathbf{w}^f\right) \cdot \nabla \mathbf{v}^f, \phi) - (p^f, \nabla \cdot \phi) \\
&= \int_{\Gamma_t^i} (\sigma^f \cdot \mathbf{n}^f) \cdot \phi \, d\gamma + \int_{\Gamma_N^f} \mathbf{h}^f \cdot \phi \, d\gamma \,, \qquad (19) \\
&(q, \nabla \cdot \mathbf{v}^f) = 0 \,, \\
&\mathbf{v}^f|_{t=0} = \mathbf{v}_0^f \,,
\end{aligned}$$

for all $\phi \in \mathbf{V}^t$ and $q \in Q^t$. Let us remark that we have kept the boundary integral term coming from the integration by parts at the interface Γ_t^i. Analogously, we define the following bilinear form

$$a^s(\mathbf{u}^s, \psi) = (\sigma^s(\mathbf{u}^\mathbf{s}), \nabla \psi) \,, \qquad (20)$$

where we have indicated with $(\cdot, \cdot)$ the $L^2(\Omega_t^s)$ inner product. Following the procedure briefly described above, we obtain at each time t, for the velocity $\mathbf{u}^s \circ \mathcal{X}^s \in \mathbf{M}_g^0$ and pressure $p^s \circ \mathcal{X}^s \in \mathbf{D}^0$, the following weak formulation for the solid problem

$$\begin{aligned}
&\rho^s(\frac{\partial^2}{\partial t^2}\mathbf{u}^s, \psi) + a^s(\mathbf{u}^s, \psi) - (p^s, \nabla \cdot \psi) = \int_{\Gamma_t^i} (\sigma^s \cdot \mathbf{n}^s) \cdot \psi \, d\gamma + \int_{\Gamma_N^s} \mathbf{h}^s \cdot \psi \, d\gamma \,, \\
&(d, \nabla \cdot \mathbf{u}^s) = 0 \,, \\
&\mathbf{u}^s|_{t=0} = \mathbf{u}_0^s \,, \qquad \mathbf{v}^s|_{t=0} = \mathbf{v}_0^s \,,
\end{aligned}$$

for all $\psi \circ \mathcal{X}^s \in \mathbf{M}^0$ and $d \circ \mathcal{X}^s \in \mathbf{D}^0$. Let us introduce a global weak formulation for the fluid-structure problem. If we define the functional space

$$\mathbf{S}^t = \{(\phi, \psi \circ \mathcal{X}^s) \in \mathbf{V}^t \times \mathbf{M}^0 : \psi|_{\Gamma_t^i} = \phi|_{\Gamma_t^i}\} \,, \qquad (21)$$

from (19), (21), (16) and (17) we can derive easily the following global formulation for every time step:

$$\begin{aligned}
&\rho^f(\frac{\partial \mathbf{v}^f}{\partial t}\Big|_{\tilde{\mathcal{A}}}, \phi) + a(\mathbf{v}^f, \phi) - \rho^f((\nabla \cdot \mathbf{w}^f)\mathbf{v}^f, \phi) + \rho^f(\left(\mathbf{v}^f - \mathbf{w}^f\right) \cdot \nabla \mathbf{v}^f, \phi) - (p^f, \nabla \cdot \phi) \\
&+ \rho^s(\frac{\partial^2}{\partial t^2}\mathbf{u}^s, \psi) + a^s(\mathbf{u}^s, \psi) - (p^s, \nabla \cdot \psi) - \int_{\Gamma_N^s} \mathbf{h}^s \cdot \psi \, d\gamma - \int_{\Gamma_N^f} \mathbf{h}^f \cdot \phi \, d\gamma = 0 \,, \\
&(q, \nabla \cdot \mathbf{v}^f) = 0 \qquad (d, \nabla \cdot \mathbf{u}^s) = 0 \,, \qquad (22) \\
&\mathbf{v}^f|_{t=0} = \mathbf{v}_0^f \qquad \mathbf{u}^s|_{t=0} = \mathbf{u}_0^s \qquad \mathbf{v}^s|_{t=0} = \mathbf{v}_0^s \,,
\end{aligned}$$

It is worth noting that by the coupling conditions (16), (17) and the particular choice of the fluid-structure test functions, the two boundary terms in the fluid and in the structure at the interface Γ_t^i cancel out. This assures that forces at the interface are correctly computed.

3 SOLUTION TECHNIQUE

In this section we explain the solution strategy used in order to solve the problem defined by (22) through the projection-penalty algorithm. Due to the saddle-point nature of the system (22), the solution is CPU-time expensive and therefore many authors have proposed different strategies to overcome this aspect. Among these, decoupled fractional step strategies are very attractive and commonly used in computational fluid dynamics (CFD) [16]. In this work we propose to split the computation of the velocity and pressure by introducing an iterative penalty-projection method. The standard projection method consists of two steps: a predictor step and a corrector one [9]. In the predictor step an intermediate velocity $\tilde{\mathbf{v}}$ that does not satisfy the divergence constraint is computed, while in the corrector step an iterative correction $\delta p_{h,proj}^{s,n+1}$ is introduced to enforce the incompressibility constraint. This projection allows us to solve the pressure and the velocity field separately but, at the same time, does not recover the original boundary conditions on pressure which are defined implicitly in the original momentum equation. This issue is relevant on solid boundaries when incompressible hyperelastic material are considered. In this case the boundary conditions involve the whole stress tensor and not only the pressure components. Setting to zero the pressure or its normal derivative in the corrector step implies always an error on the solid boundary which deforms the solid surface in the wrong way. This is particular important when large displacements are considered and moving mesh techniques are implemented.

3.1 ITERATIVE PENALTY STEP

If the projection method is applied only in the fluid domain it generates boundary error that propagates to the interior as a defective pressure wave. In some cases, due to the fluid nature of this medium, this error can be tolerated if it remains localized on small boundary layers. However in the incompressible solid case the error on the solid boundary propagates to the interior very quickly, leading to unacceptable solutions. In this work we propose to split the computation of velocity and pressure and to introduce a penalty corrections to limit the error imposed by the uncorrected boundary conditions on pressure. In order to do this we consider, in the corrector step of the projection algorithm, an iterative penalty procedure to obtain $\delta p_{h,pen}^{s,n+1}$ and enforce partially the incompressibility constraint on the boundary. The quantity $\tilde{\mathbf{v}}$ is the solution of the following momentum balance equation

$$\begin{aligned}
&\frac{\rho^f}{\Delta t}(\tilde{\mathbf{v}}_h^{f,n+1},\phi_h)_n + a(\tilde{\mathbf{v}}_h^{f,n+1},\phi_h)_n - \rho^f\Big(\big(\nabla\cdot\mathbf{w}_h^{f,n}\big)\tilde{\mathbf{v}}_h^{f,n+1},\phi_h\Big)_n \\
&\quad + \rho^f\Big(\big(\tilde{\mathbf{v}}_h^{f,n}-\mathbf{w}_h^{f,n}\big)\cdot\nabla\tilde{\mathbf{v}}_h^{f,n+1},\phi_h\Big)_n - (p_h^{f,n},\nabla\cdot\phi_h)_n - (\delta p_{h,proj}^{f,n},\nabla\cdot\phi_h)_n \\
&\qquad - (r*\delta p_{h,pen}^{f,n+1},\nabla\cdot\phi_h)_n + \frac{\rho^s}{\Delta t}(\tilde{\mathbf{v}}_h^{s,n+1},\psi_h) - \frac{\rho^s}{\Delta t}(\tilde{\mathbf{v}}_h^{s,n},\psi_h) + \Delta t\, a^s(\tilde{\mathbf{v}}_h^{s,n+1},\psi_h)
\end{aligned}$$

$$+ a^s(\mathbf{u}_h^{s,n}, \psi_h) - (p_h^{s,n}, \nabla \cdot \psi_h) - (\delta p_{h,proj}^{s,n}, \nabla \cdot \psi_h) \tag{23}$$
$$- (r * \delta p_{h,pen}^{s,n+1}, \nabla \cdot \psi_h) - \int_{\Gamma_N^s} \mathbf{h}^s \cdot \psi_h \, d\gamma - \int_{\Gamma_N^f} \mathbf{h}^f \cdot \phi_h \, d\gamma = 0 \,, \quad \forall (\phi_h, \psi_h) \in \mathbf{S}^t \,.$$

The update of the penalty correction is obtained by using

$$\delta p_{h,pen}^{n+1,it+1} = \delta p_{h,pen}^{n+1,it} + \rho * (\nabla \cdot \tilde{\mathbf{v}}) \,, \tag{24}$$

where r, ρ are real values that satisfy the relation

$$0 < r < 2\rho \,, \tag{25}$$

in order to ensure the convergence of the algorithm, [16].

3.2 PROJECTOR STEP

The projector algorithm computes the L^2 orthogonal projection of $\tilde{\mathbf{v}}_h^{n+1}$ onto the space of divergence free vectors fields H, which reads

$$\begin{aligned} \rho \frac{\mathbf{v}^{n+1} - \tilde{\mathbf{v}}^{n+1}}{\Delta t} + \nabla \delta \tilde{p}_{proj}^{n+1} = 0 \qquad & \text{in} \quad \Omega_t \,, \\ \nabla \cdot \mathbf{v}^{n+1} = 0 \qquad & \text{in} \quad \Omega_t \,. \end{aligned} \tag{26}$$

Now we reformulate this Darcy system by taking the divergence of the first expression in order to obtain a Poisson problem for $\delta \tilde{p}_{proj}^{n+1}$. This procedure is motivated by computational efficiency reasons. We use the definition of the functional space H and the L^2- orthogonality condition to define the following functional space

$$\mathbf{P}^n = \{ \zeta \in L^2(\Omega_{t^n}) : \zeta = 0 \quad \text{in} \quad \Gamma_N^f \cup \Gamma_N^s \} \,,$$

and obtain the boundary conditions for the quantity $\delta \tilde{p}_{proj}^{n+1}$. The pressure variations $\delta \tilde{p}_{h,proj}^{f,n+1} \in \mathbf{P}_h^n \subset \mathbf{P}^n$ and $\delta \tilde{p}_{h,proj}^{s,n+1} \in \mathbf{P}_h^n \subset \mathbf{P}^n$ are the solution of the following weak elliptic problem

$$(\nabla \delta \tilde{p}_{h,proj}^{f,n+1}, \nabla \zeta)_n + (\nabla \delta \tilde{p}_{h,proj}^{s,n+1}, \nabla \zeta)_n = -\frac{\rho^f}{\Delta t} (\nabla \cdot \tilde{\mathbf{v}}^{f,n+1}, \zeta)_n - \frac{\rho^s}{\Delta t} (\nabla \cdot \tilde{\mathbf{v}}^{s,n+1}, \zeta)_n \,, \tag{27}$$

for all ζ in $\mathbf{P}_h^n$. After the solution of these two sub-problems we project the predicted velocity onto the space of solenoidal vector fields that are square integrable

$$\mathbf{v}_h^{f,n+1} = \tilde{\mathbf{v}}_h^{f,n+1} - \frac{\Delta t}{\rho^f} \nabla \delta \tilde{p}_{h,proj}^{f,n+1} \qquad \text{in} \quad \Omega_t^f \,, \tag{28}$$

$$\mathbf{v}_h^{s,n+1} = \tilde{\mathbf{v}}_h^{s,n+1} - \frac{\Delta t}{\rho^s} \nabla \delta \tilde{p}_{h,proj}^{s,n+1} \qquad \text{in} \quad \Omega_t^s \,, \tag{29}$$

and we update both the pressure $p_h^{f,n+1}$ and $p_h^{s,n+1}$

$$p_h^{f,n+1} = p_h^{f,n} + \delta p_{h,proj}^{f,n+1} + \delta p_{h,pen}^{f,n+1} \qquad \text{in} \quad \Omega_t^f \,, \tag{30}$$

$$p_h^{s,n+1} = p_h^{s,n} + \delta p_{h,proj}^{s,n+1} + \delta p_{h,pen}^{s,n+1} \qquad \text{in} \quad \Omega_t^s \,. \tag{31}$$

We remark that the pressure field evaluated with this projection does not represent a correct solution near the boundaries, because here we set to zero the variation of normal pressure derivative instead of the normal component of the Cauchy stress. This leads to a wrong representation of the pressure and stress components for an incompressible solid material which tends to reduce the bending displacement field. In particular when solid domain are taken into account in the simulation such errors could lead to a wrong evaluation of the displacement field or to great instabilities. The iterative penalty correction is meant to reduce this boundary error and provide a stable behavior.

4 NUMERICAL RESULTS

In this section we present the numerical results obtained for different test cases. The computational domain is the geometry of a simple blood vessel which is under dilatation due to different inlet velocities. In particular we are interested in comparing simulations obtained with three different algorithms: a fully coupled, a simple projection and the iterative-penalty projection algorithm presented in this paper.

4.1 TEST 1

An overview of the computational domain considered is shown in Figure 2: in light gray we mark the fluid region meanwhile in dark gray the solid one. The global length of the domain is 0.1 m, its cross section is 0.01 m and the solid thickness is 0.003 m. The physical values are not realistic but they are imposed only to show easy to compare and large deformations. The density ratio between fluid and solid is considered to be

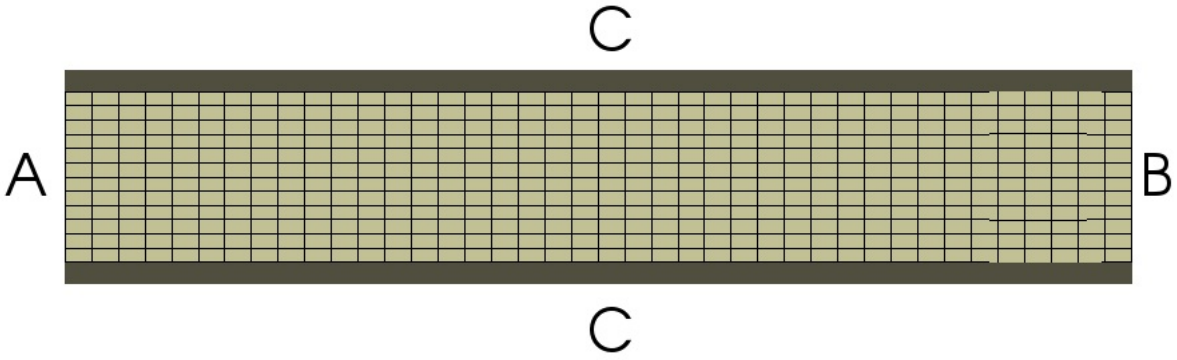

Figure 2: Test 1: Computational domain.

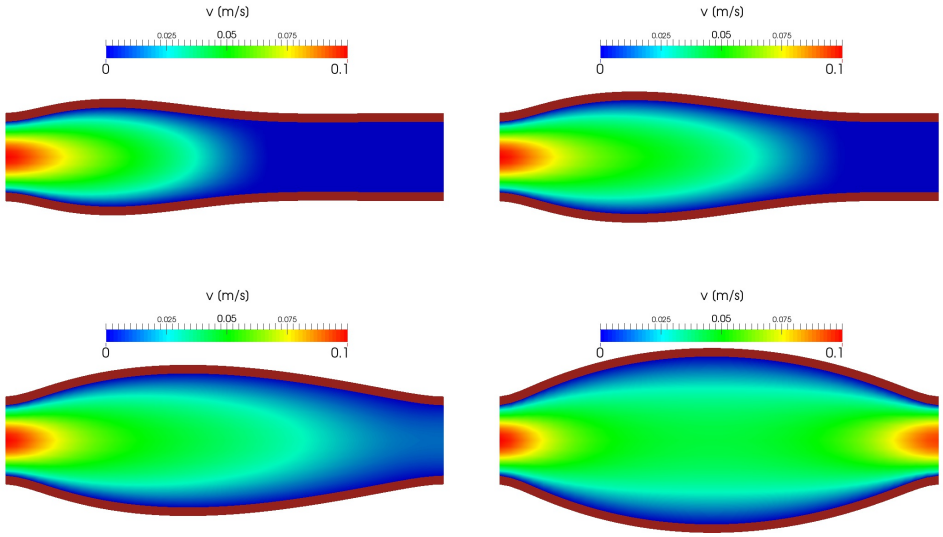

Figure 3: Test 1: Domain evolution at $t = 0.1$, 0.2, 1.5 and 10 s.

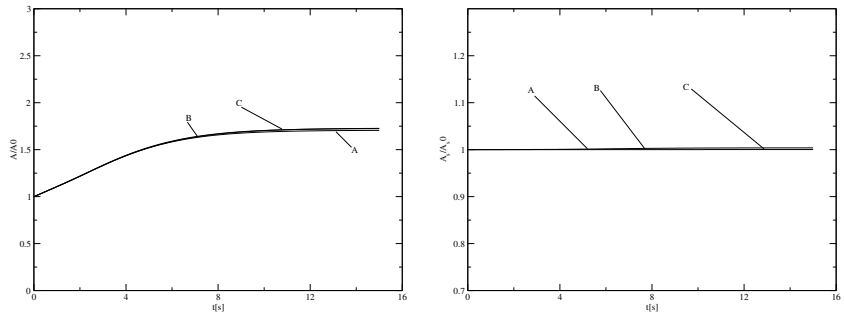

Figure 4: Test 1: Evolution over time of the global domain (left) and of the solid surface along time (right). The letters A, B and C represent the result obtained with the fully coupled, penalty-projection, projection algorithm respectively.

unitary. The dynamic fluid viscosity is set to $\mu = 0.001$ Pa s while the Young modulus E to $1000Pa$ ($\nu = 0.4$). Concerning the boundary condition of the problem, according to the nomenclature shown in Figure 2, we impose an inlet velocity equal to 0.1 m/s on the fluid region in A and a homogeneous Neumann condition on the fluid in B and C. In the solid regions B and C we impose an homogeneous Dirichlet condition. In a projection algorithm we also have to define the boundary conditions for the pressure field. We set a homogeneous Neumann condition in every boundary zone with the exception of the fluid part of B where we impose a homogeneous Dirichlet condition. An overview of the simulation is shown in Figure 3 where the velocity field at different time steps can be seen. It is worthwhile to note that the developing of the velocity field in the fluid domain causes the enlargement of the blood vessel and the steady state is reached after

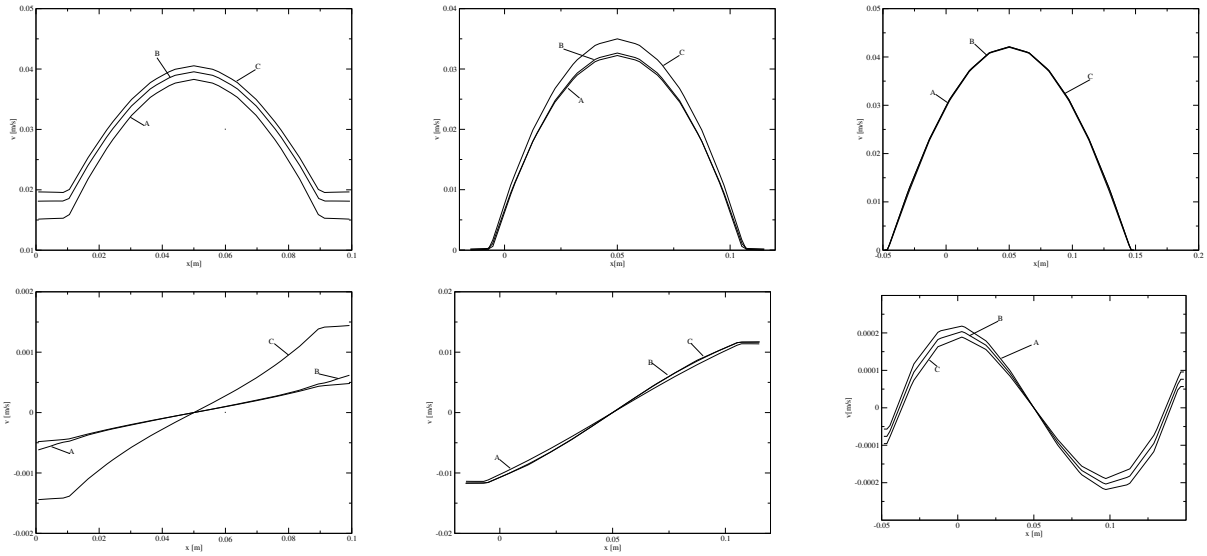

Figure 5: Test 1: Velocity field at $t = 0.1, 0.2, 4s$ in the central section of the domain, in the axial (top) and orthogonal (bottom) direction.

1.5 s (bottom right in Figure 3). We perform the same calculation using a fully coupled, simple projection and an iterative-penalty algorithm. In particular, regarding the iterative penalty method, with respect to (23) and (24) we consider $(\rho\,,\,r) = (20\,,\,1)$, that satisfies the condition (25) and ensures the convergence of the method. In the left part of Figure 4 we show the variation over time of the surface of the complete domain normalized with its initial value ($A0$). We can notice that all the methods produce quite similar results and converge to close solutions. On the right of the same figure we report the variation of the solid surface over time, normalized by its initial value (A_s0). One can observe that both three algorithms attempt to impose the incompressibility constraint and preserve the solid volume. Having a closer look to the results we can easily understand the main differences between the three methods. In Figure 5 we can observe the velocity field in the central section of the domain. The axial and transverse velocity profiles are shown on the top and bottom of Figure 5, respectively, for different time steps. We can notice that at each time step the velocity profile obtained with the iterative penalty-projection method (B) lies between the one obtained with the simple projection and the one computed with the fully pressure-velocity coupled algorithm. The difference between the curves B and C of the Figures in 5 is the iterative penalty correction which always produces a solution closer to the pressure-velocity coupled one.

4.2 TEST 2

In the second test we consider the same computational domain and physical properties of the previous case. In order to have greater deformations and test the stability of the different algorithms we impose an inlet velocity ten times greater (1 m/s). In Figure 6

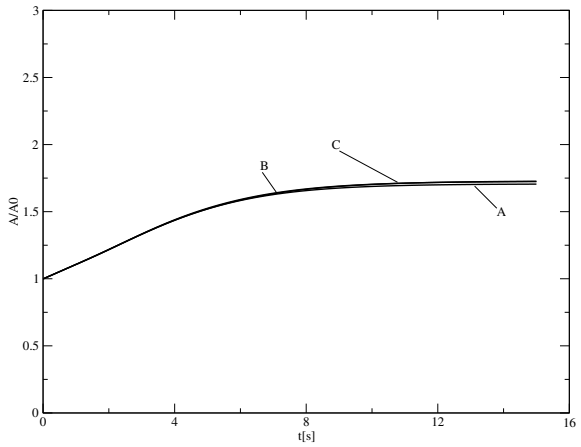

Figure 6: Test 2: Evolution over time of the domain dimension. The labels A, B and C mark the fully coupled, the penalty-projection and the simple projection algorithm respectively.

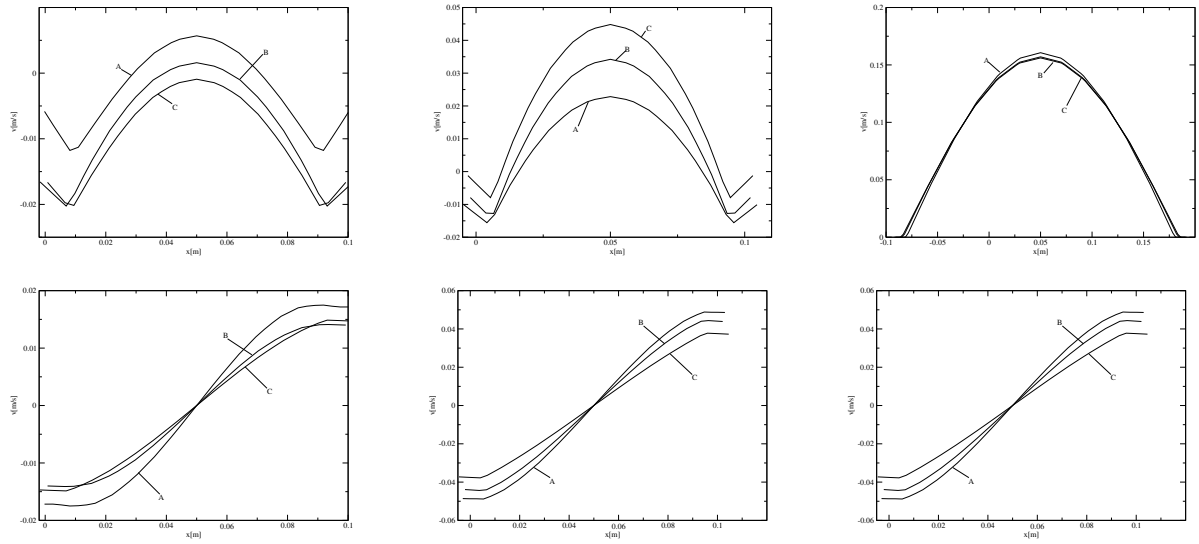

Figure 7: Test 2: Velocity field at $t = 0.1$, 0.2, 4 s along the center line: axial (top) and transverse component (bottom).

we show the normalized domain surface evolution over time. We can observe that still all the considered methods, namely the fully coupled (A), the iterative penalty-projection (B) and simple projection (C) method, reach the same steady state solution. However the volume is not conserved properly by the simple projection method. In Figure 7 we show both the axial (top) and transverse (bottom) velocity field along the center line. It is worthwhile to note that in the beginning the solution obtained with the simple projection method (curve C) is quite different from the one obtained with the fully coupled

algorithm (curve A). This is probably due to the greater velocity field. As in the previous test, comparing curve B and C of Figure 7, we can observe that the iterative penalty-projection correction (curve B) provides a better solution with respect to the one obtained with the simple projection algorithm.

5 CONCLUSION

In this work we have presented a penalty-projection algorithm for a fluid structure interaction problem. We tested the proposed method in two numerical test cases with different Reynolds numbers. The projection technique reduces the degrees of freedom of the problem and decreases the computational cost of the solution algorithm. However this solution is affected by boundary errors which propagate to the interior of the domain. The results have shown that the iterative penalty method can correct this pressure boundary error limiting its propagation inside the incompressible solid domain. A penalty-projection algorithm can be employed when the fully coupled solution of the FSI problem is not feasible due to a very high computational cost.

6 REFERENCES

[1] Razzaq, M.; Turek, S.; Hron, J.; Acker, J. F.; Numerical simulation and benchmarking of fluid-structure interaction with applications to hemodynamics, *Applied Mathematics Journal* **12**(3):123-456, 2006.

[2] Hron, J.; Turek, S.; A monolithic FEM/multigrid solver for an ALE formulation of fluid-structure interaction with applications in biomechanics. In H.-J. Bungartz and M.Schäfer, editors, *Fluid-Structure Interaction: Modelling, Simulation, Optimization*, LNCSE **53**, Springer, 2006.

[3] Bathe, K. J.; Ledezma, G. A.; Benchmark problems for incompressible fluid flows with structural interactions, *Computers & Structures* **85**:628-644, 2007.

[4] Dowell, Earl H. and Hall, Kenneth C.; Modeling of fluid-structure interaction. *Annual Review of Fluid Mechanics*, **33**(1):445-490, 2001.

[5] Hron, J.; Ouazzi, A.; Turek, S.; A computational comparison of two FEM solvers for nonlinear incompressible flow. In E. Bänsch, editor, *Challenges in Scientific Computing*, LNCSE **53**:87-109, Springer, 2002.

[6] Causin, P.; Gerbeau, J.F.; Nobile, F.; Added-mass effect in the design of partitioned algorithms for fluid-structure problems, *Computer Methods in Applied Mechanics and Engineering* **194**:4506-4527, 2005.

[7] Förster, C.; Wall, W.; Ramm, E.; Artificial added mass instabilities in sequential staggered coupling of nonlinear structures and incompressible viscous flows, *Computer Methods in Applied Mechanics and Engineering* **196**:1278-1293, 2007.

[8] Heil, M.; An efficient solver to the fully coupled solution of large-displacement fluid-structure interaction problems, *Computer Methods in Applied Mechanics and Engineering* **193**:1-23, 2004.

[9] Jobelin, M.; Lapuerta, C.; Latché, J.-C.; Angot, Ph.; Piar, B.; A finite element penalty-projection method for incompressible flows, *Journal of Computational Physics* **217**:502-518, 2006.

[10] Guermond, J.L.; Minev, P.; Shen, J.; An overview of projection methods for incompressible flows, *Computer Methods in Applied Mechanics and Engineering* **195**:6011-6045, 2006.

[11] J. Donea, S. Giuliani and J. Halleux, An Arbitrary Lagrangian Eulerian Finite Element Method for transient Fluid-Structure Interactions. *Comput. Meth. Appl. Mech. Eng.* Vol.**33**,1982, pp. 689–723.

[12] P. Tallec and J. Mouro, Fluid structure interaction with large structural displacements, *Computer Methods in Applied Mechanics and Engineering*, **190**, pp.24-25, pp. 3039-67, 2001.

[13] P.A. Sackinger, P.R. Schunk and R.R. Rao, A Newton-Raphson pseudo-solid domain mapping technique for free and moving boundary problems: a finite element implementation, *Journal of Computational Physics* **125**(1):83-103, 1996.

[14] O.C. Zienkiewicz and R.L. Taylor, *The finite element method*, McGraw Hill, (1) 1991.

[15] E. Aulisa, A. Cervone, S. Manservisi and P. Seshaiyer, A multilevel domain decomposition approach for studying coupled flow applications, *Commun. Comput. Phys.*, **6**, pp.319-341 2009.

[16] S. C. Brenner, R. Scott, The Mathematical Theory of Finite Element Methods, Texts in applied mathematics **15**, *Springer* 2008.